Article

Application of a Partially Invariant Exact Solution of the Thermosolutal Convection Equations for Studying the Instability of an Evaporative Flow in a Channel Heated from Above

Victoria B. Bekezhanova [1,2,†] and Olga N. Goncharova [2,3,*,†]

1 Department of Differential Equations of Mechanics, Institute of Computational Modeling SB RAS, 660036 Krasnoyarsk, Russia; vbek@icm.krasn.ru
2 World-Class Research Center "Advanced Digital Technologies", Tyumen State University, 625003 Tyumen, Russia
3 Institute of Mathematics and Information Technologies, Altai State University, 656049 Barnaul, Russia
* Correspondence: gon@math.asu.ru; Tel.: +7-3852-298137
† These authors contributed equally to this work.

Abstract: The characteristics of a stationary flow of a volatile liquid driven by a co-current gas flux in a flat horizontal mini-channel upon the non-zero transverse temperature drop are studied. We use an exact solution of the thermosolutal convection equations for describing the heat and mass transfer caused by the combined action of gas pumping, buoyancy, thermocapillarity and linear heating of the channel walls in a two-layer system. The influence of heating from above on the parameters of the ground state and the stability characteristics of the basic flow is explored using an example of the ethanol–air system. We evaluate the thresholds of the linear stability and select the most dangerous modes. Heating from above results in flow stabilization. Instability appears in the form of oscillatory cellular convective patterns.

Keywords: mathematical modeling; exact solution; evaporative convection; oscillatory instability

1. Introduction

Mathematical modeling of heat and mass transfer processes under the conditions of phase transitions in fluid media is a very complex problem. A commonly used approach to describe thermal convection in liquids and gases is based on the application of the fundamental conservation laws of continuum mechanics. Constitutive equations and boundary conditions on the surface dividing the media being in various aggregate states are formulated with respect to some additional presuppositions of physical chemistry and thermodynamics. When using the Navier–Stokes equations for an incompressible medium and the heat and mass transfer equations or their Boussinesq approximations, the main problem consists in the choice of a method of taking into account the phase interactions, including the formulation of conditions at the interface and the selection of the closing relations, which ensures the correctness of the problem statement. The feature of the convection equations derived on the basis of the Navier–Stokes equations is that the relations are differential expressions of the conservation laws of mass, momentum and energy and imply the natural symmetry properties of the space-time and fluid moving in this space [1]. The comprehensive review of the mathematical models of evaporative convection formulated within the framework of various approaches, summary of the underlying hypotheses, necessary characteristics and properties of interfaces and types of the mass transfer are presented in [2].

The development of mathematical models of evaporative convection includes their verification based on the results of experimental studies. The modern experimental instruments and measuring techniques allow one to investigate and quantify the velocity

and temperature fields at the interface, in the near-surface layers and inside the liquid volume. In addition, it is possible to experimentally determine the vapor content in the gas phase and the evaporation mass flow rate, even in the case where the mass transfer effects are rather slight (for example, under the diffusion-type evaporation occurring near the local thermodynamic equilibrium state). In [3–6], the experimental research methods are described, and the measurement data of various flow characteristics in the two-phase systems with the working fluids such as ethanol/HFE-7100 (liquid) and nitrogen/air (gas) are presented.

The use of the experimental methods is often limited due to the high resource costs, especially when it is necessary to repeatedly simulate the real conditions of the convective processes. In many cases, theoretical investigations are needed to obtain the preliminary characteristics of the flow regimes under various conditions, whose rapid experimental implementation is problematic, for example, for low gravity conditions. The possibility to carry out a quick theoretical analysis increases if the exact solution of the governing equations underlying the mathematical model is known. Construction of exact analytical solutions (solutions of a special form), which satisfy the boundary conditions and admit a physical interpretation for describing the process under study, in particular, convection with evaporation, is of particular interest. With the help of exact solutions, it becomes possible to reveal the nature of the dependences of the main characteristics of the system (such as the fluid flow rate, coolant temperature, vapor content in the gas phase, mass evaporation rate) on various parameters (thermophysical properties of the working media, geometric characteristics of the flow domain) and on the external impacts (the intensity of the thermal load at the boundaries and gravitational field). The study of the stability of the derived solutions will make it possible to determine the ways to control the arising flow regimes of the working fluids due to various mechanisms (see [7–11]).

The analysis of the experimental data shows that an evaporative flow is characterized by the presence of interfacial temperature inhomogeneities resulting from the decrease in the average kinetic energy of the liquid volume. The occurrence of a temperature gradient should be regarded by a solution of the corresponding problem. The Ostroumov–Birikh solution [12,13] of the Navier–Stokes equations considered in the Boussinesq approximation takes into account this effect due to the linear dependence of the temperature function on the longitudinal coordinate implied by the solution structure. Thus, the possibility of generalizing this solution to describe convection under evaporation (and condensation) conditions has been noticed. The Ostroumov–Birikh type solutions are partially invariant ones of rank 1 and defect 3 for the problem in the two-dimensional formulation. The group nature of such solutions, including their analogues for the case of thermosolutal convection, was proved in [14]. The group origin of the solutions guarantees their physical realizability and plausibility due to the symmetry properties inherited by the exact solutions. The research methodology based on the application of the exact solutions allows one to effectively study the fundamental and secondary features of the physical processes described with the help of the Navier–Stokes and heat transfer equations (or their approximations).

A variety of instability forms is peculiar to multilayer systems, since the presence of the interfaces causes the appearance of an additional factor related to the action of thermocapillary forces [15]. The instability in a two-layer fluid can be developed even in the conditions of potentially stable temperature stratification of the system [15,16]. If thermocapillary convection is accompanied by evaporation, then an additional mechanism of instability appears due to the cooling of the liquid surface. In the present paper, we examine thermocapillary bilayer flows with diffusion-limited evaporation in a plane channel under terrestrial gravity. We consider the case when thermal load distributed according to the linear law with respect to the longitudinal coordinate is applied on the channel walls. Here, the temperature of the upper wall is higher than that of the lower boundary. We use the Ostroumov–Birikh type exact solution of the thermosolutal equations [17] in order to scrutinize the characteristics of the ground state and dependence of the thresholds of linear stability on the heating conditions. A comparative analysis of the results obtained for the

cases of the non-zero transverse temperature drop and equal thermal load applied on the channel walls is performed.

2. Problem Statement

We consider liquid–gas thermocapillary flows in a flat horizontal mini-channel with fixed impermeable walls $y = -l$ and $y = h$ subjected to the linear heating in the direction of the x-axis (Figure 1). We assume that the fluids are viscous heat-conducting incompressible media divided by a smooth interface Γ. The gas in the upper layer is pumped at a given flow rate Q; it leads to a formation of additional interfacial shear stress and liquid evaporation from the surface Γ. Therefore, the overlying layer is filled with the mixture of the background gas and liquid vapor. We consider the volatile component as a non-reactive impurity.
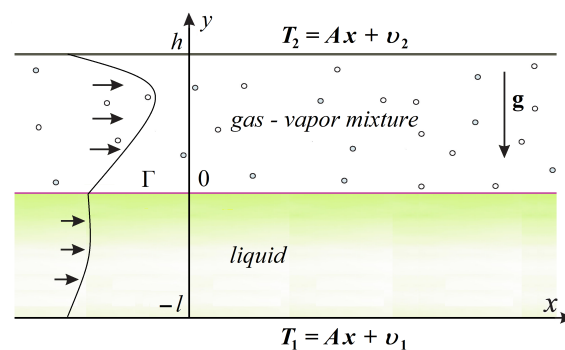
Figure 1. The model of a two-phase system with the interface in the Cartesian coordinates.

The mechanisms governing the convective flows with evaporation in the bilayer system are gas pumping, buoyancy and thermocapillary forces and linear heating of the channel walls. We use a two-sided mathematical model on the basis of the Oberbeck–Boussinesq approximation for describing the combined convection. The convective heat and mass transfer in the jth fluid is governed by the following equations

$$\frac{\partial \mathbf{v}_j}{\partial t} + (\mathbf{v}_j \cdot \nabla)\mathbf{v}_j = -\frac{1}{\rho_j}\nabla p_j + \nu_j \Delta \mathbf{v}_j - \mathbf{g}(\beta_j T_j + \delta_j^2 \gamma C),$$

$$\text{div } \mathbf{v}_j = 0, \quad \frac{\partial T_j}{\partial t} + \mathbf{v}_j \cdot \nabla T_j = \chi_j(\Delta T_j + \delta_j^2 \alpha_C \Delta C). \tag{1}$$

$$\frac{\partial C}{\partial t} + \mathbf{v}_2 \cdot \nabla C = D(\Delta C + \alpha_T \Delta T_2). \tag{2}$$

Hereinafter, the subscripts or superscripts $j = 1$ and $j = 2$ correspond to the functions and parameters related to the liquid and gas layers, respectively. Equation (2) describes the vapor transfer in the gas layer. In Equations (1) and (2), $\mathbf{v} = (u, v)$ is the velocity vector, p is the modified pressure giving a deviation of the true fluid pressure from the hydrostatic one, T is the temperature, C is the vapor concentration function, $\mathbf{g} = (0, -g)$ is the vector of the gravity force acceleration, ρ is the reference density, ν, χ, β are the coefficients of kinematic viscosity, heat diffusivity, and thermal expansion, respectively, D is the coefficient of vapor diffusion in the gas, γ is the density concentration coefficient, the parameters α_T and α_C are the Soret and Dufour coefficients, respectively, and δ_j^2 is the Kronecker delta.

On both outer boundaries, no-slip conditions for the velocity functions and the linear law of the temperature distribution are set. On the upper wall, we additionally impose the zero vapor flux condition. The boundary conditions on the channel walls are as follows:

$$y = -l, \quad u_1 = 0, \quad T_1 = Ax + \vartheta_1,$$

$$y = h: \quad u_2 = 0, \quad T_2 = Ax + \vartheta_2, \quad \frac{\partial C}{\partial y} = 0. \tag{3}$$

Here, the positive or negative values of the longitudinal temperature gradient A correspond to the heating or cooling of the walls in the direction of the x-axis, respectively. In the first case, relative heaters are arranged downstream. The latter corresponds the configuration with the heaters located at the channel inlet. The constants ϑ_j set the wall temperature. When $\vartheta_1 \neq \vartheta_2$, a transverse temperature drop is formed in the channel.

The continuity conditions for the velocity and temperature, kinematic condition and balance relations for the forces and heat are set on the common internal boundary Γ. We supplement the standard conditions with the relation specifying the concentration of saturated vapor. In the general form, the interface conditions are as follows [18]:

$$\mathbf{v}_1 = \mathbf{v}_2, \quad T_1 = T_2, \quad \mathbf{v}_1 \cdot \mathbf{n} = \mathbf{v}_2 \cdot \mathbf{n} = V_n, \quad (\mathbf{P}_1 - \mathbf{P}_2)\mathbf{n} = 2\sigma H\mathbf{n} + \nabla_{\Gamma}\sigma,$$

$$\kappa_1 \frac{\partial T_1}{\partial n} - \kappa_2 \frac{\partial T_2}{\partial n} - \alpha_C \kappa_2 \frac{\partial C}{\partial n} = -LM, \quad C = C_0(1 + \varepsilon(T_2 - T_0)), \tag{4}$$

where $\mathbf{n}$ is the unit normal vector to Γ directed from the lower layer into the upper one, V_n is the velocity of motion of the surface Γ in the direction of the normal $\mathbf{n}$ ($V_n = -f_t/|\nabla_x f|$, $\nabla_x f = (f_x, f_y, f_z)$, $f(x, y, z, t) = 0$ is the implicit equation of the interface, in the stationary case $V_n = 0$), $\mathbf{P}_j = -p_j\mathbf{I} + 2\nu_j\rho_j\mathbf{D}(\mathbf{v}_j)$ is the stress tensor in the jth medium, $\mathbf{I}$ is the unit tensor, $\mathbf{D}(\mathbf{v}_j) = (\nabla\mathbf{v}_j + (\nabla\mathbf{v}_j)^*)/2$ is the velocity-strain tensor of the vector field $\mathbf{v}_j$, H is the mean curvature of Γ (if the surface Γ is bent outwards, then $H > 0$), ∇_{Γ} is the vector differential operator $\nabla_{\Gamma} = \nabla - \mathbf{n}(\mathbf{n} \cdot \nabla)$, σ is the surface tension of the liquid, $\sigma = \sigma_0 - \sigma_T(T_1 - T_0)$, σ_0 is the reference value of the surface tension at the equilibrium temperature temperature T_0, κ_j is the heat conductivity coefficient, L is the latent heat of evaporation, M is the mass flow rate of vaporization, C_0 is the equilibrium concentration of the saturated vapor, $\varepsilon = L\mu/(R^*T_0^2)$, μ is the molar mass of the evaporating liquid, and R^* is the universal gas constant.

The intensity of gas pumping is determined by the condition specifying the gas flow rate in the upper layer:

$$Q = \int_0^{h_2} \rho_2 u_2(y)\, dy. \tag{5}$$

Equations (1) and (2) supplemented by conditions (4) represent the basis of the full two-sided model for describing convection in the two-phase system under the conditions of the diffusive type evaporation through the interface [2]. Possible variants of the conditions on the outer boundaries of the flow domain within the framework of the model are discussed in [17].

3. Form of the Exact Solution

Due to the group properties of systems (1) and (2), we can find their solution in a special form [10,17]:

$$u_j = u_j(y), \quad v_j = 0, \quad T_j = T_j(x, y) = (a_1^j + a_2^j y)x + \vartheta_j(y),$$

$$C = C(x, y) = (b_1 + b_2 y)x + \phi(y), \quad p_j = p_j(x, y). \tag{6}$$

Here, a_k^j, b_k ($k = 1, 2$) are the solution parameters. Solution (6) belongs to the Birikh solution class and has a group origin [19]. It describes steady flows in a two-layer system where one of the fluids is a binary mixture.

Substituting the required functions in form (6) into (1)–(5), we find that the solution exactly satisfies all the governing equations and boundary conditions. Here, the time invariance of the solution ensures that the kinematic condition is identically satisfied. Projecting the dynamic condition on $\mathbf{n}$, we obtain the equality $H = 0$. It means that the surface Γ remains non-deformed, and the equation $y = 0$ defines the interface position. The continuity condition for the temperature on Γ imposes the equality $a_1^j = A$, so that the

temperature in the jth layer is defined by the function $T_j = (A + a_2^j)x + \vartheta_j(y)$. The value of the temperature gradient on the interface coincides with the given value of the boundary gradient A. Here, the interfacial gradient governs the surface tension-driven convection and evaporation intensity. We do not consider the case $A = 0$, since in this situation exact solution (6) degenerates into a simpler one with the zero constants a_k^j, b_k ($k = 1, 2$). The latter does not belong to the Birikh solution class. Moreover, it does not take into account the impact of the thermocapillarity.

Lastly, if the linear heating with equal boundary gradients is applied on the channel walls, then only the case $M = \text{const}$ can be realized due to the solution form [17]. The condition means that evaporation at the interface occurs at a constant rate along the whole length of the channel. We use the mass balance condition for evaluating the evaporation rate M:

$$M = -D\rho_2\left(\frac{\partial C}{\partial n} + \alpha_T \frac{\partial T_2}{\partial n}\right). \tag{7}$$

If $M > 0$, then there occurs evaporation of the liquid into the carrier gas. The case of $M < 0$ describes the vapor condensation from the gas phase.

Direct integration of Equations (1) and (2) allows one to find explicit expressions for all the required functions. Considering the above, we obtain the following polynomial form for functions (6):

$$
\begin{aligned}
u_j(y) =\ & c_3^j + c_2^j y + c_1^j \frac{y^2}{2} + L_3^j \frac{y^3}{6} + L_4^j \frac{y^4}{24}, \\[6pt]
p_j(x, y) =\ & \left(d_1^j + d_2^j y + d_3^j \frac{y^2}{2}\right)x + c_8^j + K_1^j y + K_2^j \frac{y^2}{2} + K_3^j \frac{y^3}{3} + K_4^j \frac{y^4}{4} + \\[4pt]
& + K_5^j \frac{y^5}{5} + K_6^j \frac{y^6}{6} + K_7^j \frac{y^7}{7} + K_8^j \frac{y^8}{8}, \\[6pt]
T_j(x, y) =\ & \left(A + a_2^j y\right)x + c_5^j + c_4^j y + N_2^j \frac{y^2}{2} + N_3^j \frac{y^3}{6} + N_4^j \frac{y^4}{24} + \\[4pt]
& + N_5^j \frac{y^5}{120} + N_6^j \frac{y^6}{720} + N_7^j \frac{y^7}{1008}, \\[6pt]
C(x, y) =\ & (b_1 + b_2 y)x + c_7 + c_6 y + S_2 \frac{y^2}{2} + S_3 \frac{y^3}{6} + S_4 \frac{y^4}{24} + \\[4pt]
& + S_5 \frac{y^5}{120} + S_6 \frac{y^6}{720} + S_7 \frac{y^7}{1008}.
\end{aligned}
\tag{8}
$$

The algorithm for the calculation of all the unknown constants and solution parameters can be found in [17]. Therein, the physical interpretation of the exact solution is given, and the conditions of its applicability for describing real physical systems are specified.

4. Influence of the Heat from Above on the Convective Regime

We consider ethanol–air as a working two-phase system. The physical parameters of the media and equilibrium value of the vapor concentration corresponding to the equilibrium temperature $T_0 = 293.15$ K are listed in Table 1. The system is in the field of mass forces with $g = 9.81 \text{ m/s}^2$. We examine the case when the thicknesses of the liquid and gas layers, gas flow rate and average temperature of the lower wall are fixed: $l = 3$ mm, $h = 5$ mm, $Q = 9.6 \times 10^{-6}$ kg/(m·s), $\vartheta_1 = 293.15$ K. The temperature gradient A ranges from -5 to 5 K/m. We model the heat from above by means of a change in the value ϑ_2, so that $\vartheta = \vartheta_2 - \vartheta_1$ characterizes the intensity of the top heating. We consider the configurations where the average temperature of the upper wall ϑ_2 ranges from 293.15 to 295.15 K, i.e., the values of ϑ do not exceed 2 degrees. These values of A and ϑ_2 provide moderate temperature drops in the whole system, thereby ensuring the correct application of the Oberbeck–Boussinesq approximation in the problem under study. We track the changes in the interface velocity u_Γ, temperature drop in the system $\triangle T$ and evaporation

rate M, which are caused by the variation in the intensity of the external temperature action. Table 2 presents the values of the specified characteristics for some cases.

Table 1. Physicochemical parameters of the ethanol–air two-phase system [20,21].

| Parameter	Ethanol (Liquid)	Air (Gas)
Density ρ, kg/m^3	0.79×10^3	1.205
Kinematic viscosity ν, m^2/s	0.15×10^{-5}	0.15×10^{-4}
Thermal expansion β, K^{-1}	1.08×10^{-3}	3.67×10^{-3}
Heat diffusivity χ, m^2/s	0.38×10^{-7}	0.21×10^{-4}
Heat conductivity κ, W/(m·K)	16.72×10^{-2}	2.62×10^{-2}
Molar mass μ, kg/mol	46×10^{-3}	29×10^{-3}
Temperature coefficient of the surface tension σ_T, N/(m·K)	0.8×10^{-4}	
Surface tension at the equilibrium temperature σ_0, N/m	22.03×10^{-3}	
Laten heat of vaporization L, W·s/kg	8.79×10^5	
Coefficient of vapor diffusion D, m^2/s		1.35×10^{-5}
Concentration expansion γ		-0.62
Dufour coefficient α_c, K		10^{-3}
Soret coefficient α_T, K^{-1}		5×10^{-3}
Equilibrium vapor concentration C_0		0.1

Table 2. The values of the convective regime characteristics (u_Γ, mm/s; $\triangle T$, K; M, kg/(m^2·s)) for the ethanol–air system at various intensities of the external temperature action.

| A, K/m	$\vartheta_2 = 293.15$ K	$\vartheta_2 = 294.15$ K	$\vartheta_2 = 295.15$ K
-5	$u_\Gamma = 0.943$ $\triangle T = 0.52$ $M = 3.982 \times 10^{-6}$	$u_\Gamma = 0.943$ $\triangle T = 1.25$ $M = -7.705 \times 10^{-6}$	$u_\Gamma = 0.943$ $\triangle T = 2.25$ $M = -1.939 \times 10^{-5}$
-1.5	$u_\Gamma = 0.376$ $\triangle T = 0.11$ $M = 4.675 \times 10^{-7}$	$u_\Gamma = 0.376$ $\triangle T = 1.075$ $M = -1.122 \times 10^{-5}$	$u_\Gamma = 0.376$ $\triangle T = 2.075$ $M = -2.291 \times 10^{-5}$
1.5	$u_\Gamma = -0.110$ $\triangle T = 0.081$ $M = 1.557 \times 10^{-7}$	$u_\Gamma = -0.110$ $\triangle T = 1.075$ $M = -1.153 \times 10^{-5}$	$u_\Gamma = -0.110$ $\triangle T = 2.075$ $M = -2.322 \times 10^{-5}$
5	$u_\Gamma = -0.678$ $\triangle T = 0.428$ $M = 2.943 \times 10^{-6}$	$u_\Gamma = -0.678$ $\triangle T = 1.25$ $M = -8.745 \times 10^{-6}$	$u_\Gamma = -0.678$ $\triangle T = 2.25$ $M = -2.043 \times 10^{-5}$

We note that the constants determining the velocity functions in the layers do not depend on the values ϑ_j. Therefore, the presence of the non-zero transverse temperature drop does not lead to the alteration of the velocity field, and hence to the formation of topologically new types of flows. It is sufficient to compare the velocity profiles corresponding to various values of ϑ_2 at the same gradients A in Figures 2 and 3 and the values of the interface velocity u_Γ given in Table 2. All possible classes of bilayer evaporative flows and mechanisms governing certain flow regimes are described in detail in [17]. With all the fixed parameters of the system, the temperature driving factor resulting in the transformation of the velocity profile is related only to changes in the temperature gradient A. The sign and value of the interface gradient A determine the direction and intensity of the Marangoni force action, respectively. The liquid moves from the hot domain into the region with a lower temperature along the interface due to the thermocapillary effect. Depending on the values of A, we observe the transition from the mixed type flows (the corresponding velocity profiles are shown in Figures 2a,d and 3a,d to the purely thermocapillary regime (Figures 2g and 3g). Here, the intensity of the surface flow grows with an increase in $|A|$ (compare the values u_Γ at various A in Table 2).
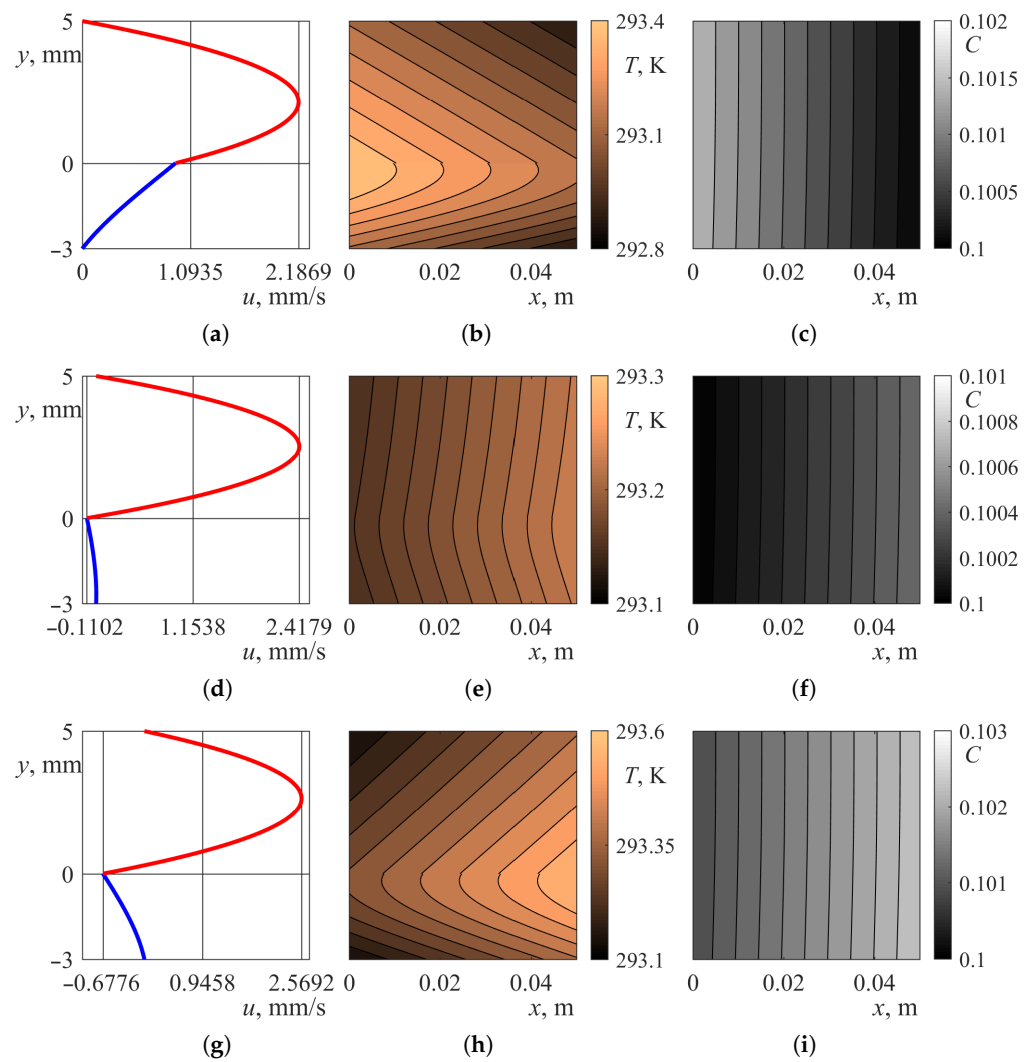
Figure 2. The velocity field (**left column**), temperature isolines (**middle column**) and concentration isolines (**right column**) at $\vartheta_2 = 293.15$ K: mixed type flow, $A = -5$ K/m (**a–c**); mixed type flow, $A = 1.5$ K/m (**d–f**); purely thermocapillary flow, $A = 5$ K/m (**g–i**).
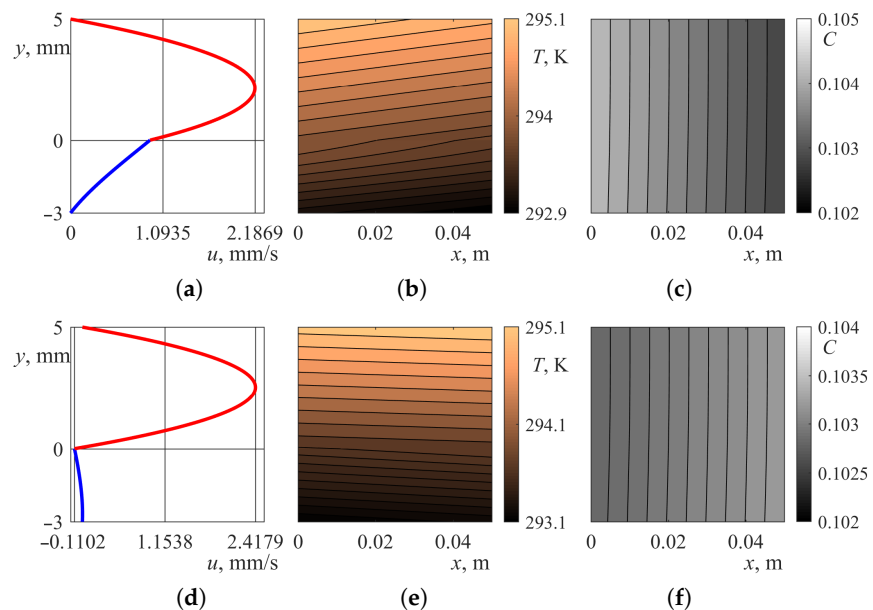
Figure 3. *Cont.*
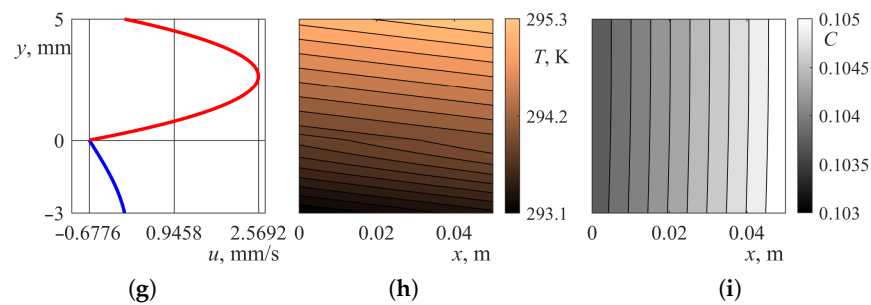
Figure 3. The velocity field (**left column**), temperature isolines (**middle column**) and concentration isolines (**right column**) at $\vartheta_2 = 295.15$ K: mixed type flow, $A = -5$ K/m (**a–c**); mixed type flow, $A = 1.5$ K/m (**d–f**); purely thermocapillary flow, $A = 5$ K/m (**g–i**).

If an equal thermal load is applied on the channel walls, we have $M > 0$ (Table 2, the case $\vartheta_2 = 293.15$ K), i.e., the liquid evaporates into the carrier gas. Here, regimes with the near-surface thermocline are realized. The feature of these regimes is that the liquid in the lower layer has stable temperature stratification, whereas the gas layer is unstably stratified (Figure 2b,e,h). The heat from above essentially influences not only the pattern of the thermal field but also the regime of phase transition. We can observe the formation of the totally stable temperature field in the bilayer system (Figure 3b,e,h). In this state, the thermal equilibrium is upset since the temperature of the liquid vapor is higher than the temperature within the volume liquid phase along the entire length of the channel. Here, the vapor concentration in the background gas exceeds the equilibrium value C_0 within the whole upper layer (compare the variation ranges of the C function in Figures 2 and 3). It means that the chemical equilibrium imposed by the condition providing the saturated vapor concentration at the interface is also upset. Since the system always tends to remain in the equilibrium state, then there occurs the condensation of vapor from the gas phase into the liquid. The solution correctly describes such a change of the phase transition regime, predicting negative values of the M parameter (Table 2). The increase or decrease in the vapor content along the channel completely depends on the direction of the thermocapillary effect, entailing the heat transfer on the phase boundary. If the interface temperature drops along the x-axis ($A < 0$), then the vapor concentration in the gas diminishes (see Figures 2b,c and 3b,c). With an increase in the interface temperature ($A > 0$), the vapor content grows (see, for example, Figures 2h,i and 3h,i).

We found that even rather little heat from above results in a drastic change-over of the evaporative convection regime. Therefore, we can expect that such an additional temperature impact affects the stability properties of the modes. Further, we will investigate the linear stability of the basic state described by exact solution (6).

5. Linearized Stability Problem

We move on to dimensionless variables to formulate the stability problem and to introduce the governing similarity criteria. The values of physical parameters of the gas are chosen as reference ones for the corresponding characteristics. Then, a dimensionless analogue $\widehat{\omega}_j = \omega_j / \omega_2$ corresponds to each physical parameter ω_j. Since $\widehat{\omega}_2 = 1$ for all the parameters, below we omit the "circumflex" symbol for the physical characteristics. The gas layer thickness h is taken as a characteristic size, and $\widehat{h} = l/h$ denotes the non-dimensional height of the liquid layer. We use the values of ν_2/h, $\rho_2 \nu_2^2/h^2$ and Ah as scales of velocity, pressure and temperature, respectively. Then, the dimensionless variables of time and space are $\tau = \nu_2 t/h^2$ and $\boldsymbol{\xi} = (\xi, \eta) = (x/h, y/h)$. We use the notations $\widehat{\alpha}_C = \alpha_C/Ah$ and $\widehat{\alpha}_T = \alpha_T/(Ah)$ for the dimensionless Dufour and Soret coefficients, respectively. The concentration function C does not require non-dimensionalization. The following dimensionless parameters and similarity criteria are introduced:

$$\text{Gr} = \frac{g\beta_2 A h^4}{\nu_2^2}, \quad \text{Pr} = \frac{\nu_2}{\chi_2}, \quad \text{Ga} = \frac{gh^3}{\nu_2^2}, \quad \text{Sc} = \frac{\nu_2}{D},$$
$$\text{Ma} = \frac{\sigma_T A h^2}{\nu_2^2 \rho_2}, \quad \text{E} = \frac{LD\rho_2}{\kappa_2 Ah}. \tag{9}$$

Here, Gr, Pr, Ga, Sc, Ma are the Grashof, Prandtl, Galilei, Schmidt and Marangoni numbers respectively, and E is the evaporation number.

For the stability studies, we assume that the basic state is perturbed by infinitesimally small disturbances that are represented as

$$\mathbf{V}_j(\xi, \tau) = (U_j(\eta), V_j(\eta)) \exp[i(\alpha_x \xi - \lambda \tau)], \quad P_j(\xi, \tau) = P_j(\eta) \exp[i(\alpha_x \xi - \lambda \tau)],$$

$$\Theta_j(\xi, \tau) = \Theta_j(\eta) \exp[i(\alpha_x \xi - \lambda \tau)], \quad S(\xi, \tau) = S(\eta) \exp[i(\alpha_x \xi - \lambda \tau)],$$

where α_x is the dimensionless wave number along the x-axis, $\lambda = \lambda_r + i\lambda_i$ is the complex time decrement. We assume that the interface Γ remains to be non-deformed when subjected to the perturbations. The possibility to keep the flatness of the interface between the evaporating liquid and the overlaying gas flux can be realized in real physical conditions. A detailed description of the experimental technique using the optical shadowgraph method that allows one to control the non-deformed position of the flat phase boundary with the accuracy of ± 10 μm is given in [5].

Linearizing governing Equations (1) and (2) and boundary conditions (3) and (4) near stationary solution (6), we obtain the following problem:

$$-\widehat{h} < \eta < 0: \quad (-i\lambda + i\alpha_x u_1)U_1 + u_1' V_1 = -i\alpha_x \rho^{-1} P_1 + \nu(U_1'' - \alpha_x^2 U_1),$$

$$(-i\lambda + i\alpha_x u_1)V_1 = -\rho^{-1} P_1' + \nu(V_1'' - \alpha_x^2 V_1) + \beta\text{Gr}\,\Theta_1, \quad i\alpha_x U_1 + V_1' = 0,$$

$$(-i\lambda + i\alpha_x u_1)\Theta_1 + U_1 T_{1\xi} + V_1 T_{1\eta} = \chi\text{Pr}^{-1}(\Theta_1'' - \alpha_x^2 \Theta_1),$$

$$0 < \eta < 1: \quad (-i\lambda + i\alpha_x u_2)U_2 + u_2' V_2 = -i\alpha_x P_2 + (U_2'' - \alpha_x^2 U_2), \tag{10}$$

$$(-i\lambda + i\alpha_x u_2)V_2 = -P_2' + (V_2'' - \alpha_x^2 V_2) + \text{Gr}\,\Theta_2 + \gamma\text{Ga}\,S, \quad i\alpha_x U_2 + V_2' = 0,$$

$$(-i\lambda + i\alpha_x u_2)\Theta_2 + U_2 T_{2\xi} + V_2 T_{2\eta} = \text{Pr}^{-1}(\Theta_2'' - \alpha_x^2 \Theta_2 + \widehat{\alpha}_C(S'' - \alpha_x^2 S)),$$

$$(-i\lambda + i\alpha_x u_2)S + U_2 C_\xi + V_2 C_\eta =$$

$$= \text{Sc}^{-1}(S'' - (\alpha_x^2 + \alpha_z^2)S + \widehat{\alpha}_T(\Theta_2'' - (\alpha_x^2 + \alpha_z^2)\Theta_2)),$$

$$\eta = -\widehat{h}: \quad U_1 = V_1 = \Theta_1 = 0,$$
$$\eta = 1: \quad U_2 = V_2 = \Theta_2 = S' = 0, \tag{11}$$

$$\eta = 0: \quad U_1 = U_2, \quad V_1 = V_2 = 0, \quad \Theta_1 = \Theta_2,$$

$$U_2' - \nu\rho U_1' + i\alpha_x(V_2 - \nu\rho V_1) = \text{Ma}\,i\alpha_x\Theta_1, \tag{12}$$

$$P_1 - P_2 = 2(\nu\rho V_1' - V_2'), \quad \kappa\Theta_1' - \Theta_2' - \widehat{\alpha}_C S' = \text{E}(S' + \widehat{\alpha}_T\Theta_2'),$$

where the prime denotes differentiation on the η-variable. System (10)–(12) presents the generalized eigenvalue problem $\lambda\mathbf{G}(\mathbf{V}, P, \Theta, S)^T = \mathbf{J}(\mathbf{V}, P, \Theta, S)^T$ for the decrement λ and the perturbation vector $(\mathbf{V}, P, \Theta, S)$, which is the corresponding eigenvector. Here, $\mathbf{G}$ is the diagonal matrix and $\mathbf{J}$ is the Jacobian matrix defining the right-hand side of the linearized problem. The diagonal elements of the $\mathbf{G}$ matrix corresponding to the time derivatives of $(\mathbf{V}, \Theta, S)$ are equal to $-i$, whereas the elements corresponding to P as well as the components related to the boundary conditions are zeros. Then, $det\mathbf{G} = 0$ and the generalized eigenvalue problem cannot be reduced to the standard one. Problem (10)–(12) is numeri-

cally solved. The numerical approach is based on the Abramov–Godunov algorithm [22], which was adapted for the case of a domain with an internal interface.

The two-phase flow described by solution (6) is unstable if at least one eigenvalue λ with a positive imaginary part exists. The instability threshold is determined by the condition $\lambda_i = 0$. Here, the eigenvalue with the largest imaginary part and the corresponding eigenvector are referred to as leading. The real part λ_r defines the oscillation frequency; if $\lambda_r = 0$, then the perturbations are monotonous. The phase velocity of the traveling waves is determined according to the formula $\omega_p = \lambda_r / \alpha_x$.

6. Instability Thresholds and Selection of Convective Patterns

In fact, the instability threshold is defined as a set of governing parameters (9) at which the leading eigenvalue crosses the real axis. Since we consider changes in the flow characteristics caused by the thermal action, then we choose the Gr and Ma numbers as key similarity criteria related to two different mechanisms of instability, namely, to the convective and thermocapillary ones. Thus, the solution of the spectral problem is reduced to finding neutral curves $\mathrm{Gr}(\alpha_x)$, determining the instability domains in the plane $(\mathrm{Ma}, \mathrm{Gr})$ and to investigating their evolution, depending on changes in ϑ.

In Figure 4a, the neutral curves $\mathrm{Gr}(\alpha_x)$ are presented. For the curve *1* calculated for the case of the equal temperature load with $\vartheta = 0$, the instability domain U_0 is to the right of the graph. The lines 2^+ and 2^- present two branches of the neutral curve plotted for the case of the top heating at $\vartheta = 1$. We use the notations U_1^+ and U_1^- to indicate the instability domains lying above and below the corresponding branch. The superscripts $+$ and $-$ correspond to the positive and negative values of the Grashof number, respectively. The values of Gr lying on the curves define the threshold values. Knowing the critical values and taking into account the relation between A and Gr (see (9)), we can evaluate the values of the temperature gradient A at which the loss of stability of the convective flow occurs. Both branches of the neutral curve obtained at $\vartheta = 2$ corresponding both to the positive and negative Grashof number provide the values of the gradient A at which the temperature drop in the whole system cannot be regarded as moderate. Therefore, we do not present the curves in the figure.
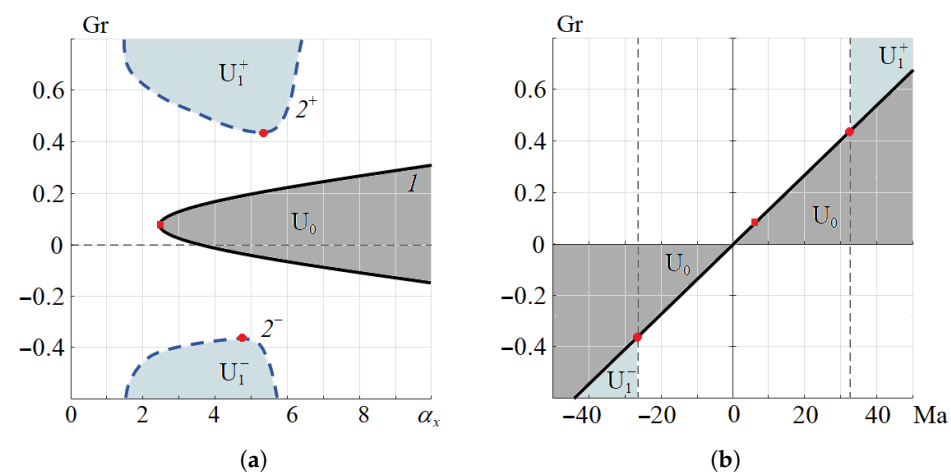

Figure 4. The neutral curves $\mathrm{Gr}(\alpha_x)$ (**a**) and instability domains on the plane $(\mathrm{Ma}, \mathrm{Gr})$ (**b**). Curves 1 and 2 correspond to the cases $\vartheta = 0$ and $\vartheta = 1$, respectively. The shaded regions U_0 and U_1 present the instability domains at $\vartheta = 0$ and $\vartheta = 1$, respectively.

We see that, at $\vartheta = 0$, there are always perturbations causing the instability of the basic flow even at small Gr. The critical value of the wave number for the most dangerous disturbance (i.e., the minimum wave number of the perturbation resulting in the stability loss) is $\alpha_{x0}^* = 2.48$, and the corresponding threshold value of the Grashof number is $\mathrm{Gr}_0^* = 0.08$. The typical form of the leading disturbance is presented in Figure 5a. We show the pattern of the temperature and hydrodynamical perturbations. The instability appears

in the form of cellular convection accompanied by the development of thermal structures with typical cores localized near the liquid–gas surface. The concentration disturbances are determined by the thermal ones. We observe the formation of alternate concentration spots or strips (depending on the length of the perturbation wave) with the elevated and reduced vapor content above the "cold" and "hot" thermal perturbations, correspondingly.

　　As seen in Figure 4, the stable temperature stratification does not guarantee the stability of the ground state. The neutral curve for the case $\vartheta = 1$ consists of two parts (Figure 4a). The extremes of the upper and lower branches have the coordinates $(\alpha_{x1}^{*+}, \mathrm{Gr}_1^{*+}) = (5.34, 0.434)$ and $(\alpha_{x1}^{*-}, \mathrm{Gr}_1^{*-}) = (4.82, -0.366)$, respectively. Thus, at $\vartheta = 1$ and $\mathrm{Gr} \in (\mathrm{Gr}_1^{*-}, \mathrm{Gr}_1^{*+})$ the formation of stable regimes is possible within the range of the wave number values under consideration. We can conclude that thermal pumping from the side of the upper wall stabilizes the flow.
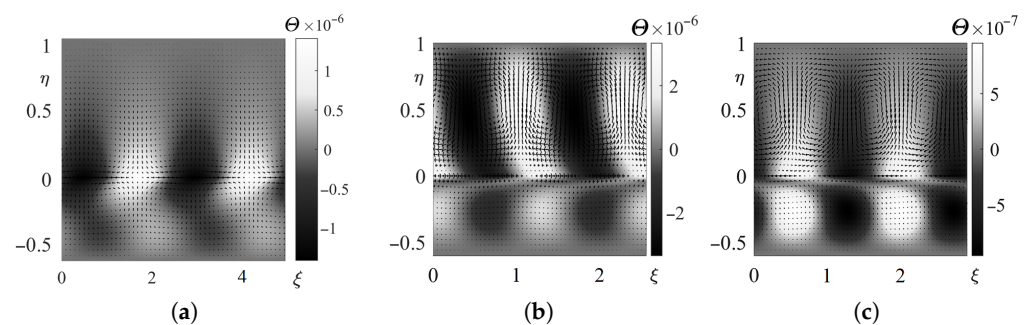
Figure 5. The pattern of the leading perturbations in the instability domains U_0 (**a**), U_1^- (**b**) and U_1^+ (**c**).

　　The development of instability in the bilayer system is always related to the action of the thermocapillary effect (Figure 4b). At small Gr and Ma (and hence at low A), if there arises a small thermal perturbation near the interface, then converging and divergent horizontal motion are formed within both phases in the domains of "cold" and "hot" thermal spots, respectively, due to the Marangoni effect. Owing to the media continuity, the fluid in the gas layer moves upward over the "cold" spot, whereas a downflow appears over the "hot" zone. The typical form of instability corresponding to this instability mechanism is presented in Figure 5a. We note that a similar type of the instability can also be realized in the bilayer system heated from above. Here, ascendant currents in the upper layer carry the cold fluid (since the temperature of the lower liquid is lower). It leads to a further decrease in temperature over the "cold" spot. Descending from the hotter wall, the fluid is heated even more, which results in the intensification of the "hot" spot, and hence in the intensification of the horizontal motion.

　　With an increase in Gr and Ma, the regimes with a thermocline near the interface are formed. Then, another mechanism causes instability. In such modes, the liquid has a stable temperature stratification when the interface temperature is higher than the substrate temperature, whereas an unstable stratification is formed in the entire gas layer. There occurs heat-gravitational convection in the gas. Due to the medium continuity, the near-surface motion results from the convective mass exchange. It generates a thermal perturbation on the interface. The liquid spreads from the perturbed "hot" thermal spot into the "cold" zone. Thus, the flow loses its stability due to the combined action of the convective and thermocapillary mechanisms. The first mechanism forms a convecting zone, whereas the second one causes the horizontal motion on the interface where small thermal perturbations arise.

　　In all the cases, we find that all the eigenvalues λ have a nonzero real part λ_r, i.e., the oscillatory instability regimes are realized in the two-phase system. The phase velocities ω_p in mm/s for the arising perturbations at various intensities of the top heating are given in Table 3. The phase velocity is calculated only for the normal waves which cause the instability of the ground flow described by the exact solution under study. These

disturbances are characterized by the wave numbers α_x, for which there are the instability domains (see domains U_0 and $U_1^{\pm}$ in Figure 4a). We present the phase velocity for the disturbances with the integer values of α_x to evaluate the character of changes in the wave characteristics. As noted earlier, the phase velocity is determined based on the values of the real part λ_r of the complex decrement λ. The presence of two values of ω_p means that two various perturbations with the same wavelength appear, but they propagate in the flux with different phase velocities and differently interact with the basic flow. We see that the temperature pumping results in the growth of the phase velocity (the values of ω_p at $\vartheta = 1$ are higher than those obtained for the case $\vartheta = 0$). The perturbations with $\omega_p < 0$ propagate in the direction opposite to the gas pumping. The drift direction is determined by the pattern of the basic flow. If the near-surface reverse flow caused by the Marangoni effect in the liquid layer is realized (see the examples of the regime in Figures 2d,g and 3d,g), then the disturbances are driven by the basic flow in the direction opposite to the x-axis (Figure 5c). When the interface liquid flow is co-directed to the gas flux (see the velocity field in Figures 2a and 3a), then the perturbations propagate down the stream and their phase velocity ω_p is positive (Figure 5b). With the negative Gr, the top heating provides conditions for the change in the drift direction of the arising patterns. In both cases, the perturbations are deformed by the basic flow. We note that the realization of the oscillatory instability in the evaporating liquids is confirmed by the experiments [23,24]. Moreover, the regimes of the spatial instability with transverse rolls drifting upstream were observed in a real two-phase system where the evaporating liquid was driven by the co-current gas flux [25].

Table 3. The values of the phase velocity ω_p, mm/s, at various temperature drops ϑ, K, for the ethanol–air system with $l = 3$ mm.

α_x	1	2	3	4	5	6	7	8	9	10
$\vartheta = 0$			0.037	0.019	0.012	−0.02	−0.054	−0.101	−0.154	−0.204
			0.101	0.132	0.171	0.194	0.237	0.283	0.319	0.397
$\vartheta = 1$				1.816	1.012	0.471	0.119			
		−6.512	−4.195	−2.107	−0.92	−0.216				

7. Conclusions

With the help of the exact solution under study, we established the stabilizing effect of top heating, obtained the threshold characteristics of the convective stability and specified the forms of the leading disturbances for the two-phase system with evaporation. The instability in this system appears in the form of oscillatory cellular convection. The regimes of instability are characterized by the presence of transversal waves traveling windward or streamwise, depending on the type of the basic flow. Based on the obtained results, we conclude that it is possible to control the convective regimes by means of the minimized top heating in order to provide the stability of the basic flow.

Author Contributions: Conceptualization, methodology, formal analysis, V.B.B. and O.N.G.; software, visualization, V.B.B.; validation, writing—original draft preparation, writing—review and editing, V.B.B. and O.N.G. All authors have read and agreed to the published version of the manuscript.

Data Availability Statement: Not applicable.

Conflicts of Interest: The authors declare no conflict of interest.

References

1. Andreev, V.K.; Kaptsov, O.V.; Pukhnachov, V.V.; Rodionov, A.A. *Applications of Group Theoretical Methods in Hydrodynamics*; Kluwer Academic Publishers: Dordrecht, The Netherlands; Boston, MA, USA; London, UK, 1998; 408p.
2. Bekezhanova, V.B.; Goncharova, O.N. Problems of the Evaporative Convection (Review). *Fluid Dyn.* **2018**, *53* (Suppl. S1), S69–S102. [CrossRef]
3. Lyulin, Y.; Kabov, O. Evaporative convection in a horizontal liquid layer under shear-stress gas flow. *Int. J. Heat Mass Transfer* **2014**, *70*, 599–609. [CrossRef]
4. Machrafi, H.; Lyulin, Y.; Iorio, C.S.; Kabov, O.; Dauby, P.C. Numerical parametric study of the evaporation rate of a liquid under a shear gas flow: Experimental validation and the importance of confinement on the convection cells and the evaporation rate. *Int. J. Heat Fluid Flow* **2018**, *72*, 8–19. [CrossRef]
5. Lyulin, Y.; Kabov, O.A. Thermal effect in the evaporation process from the interface of the horizontal liquid layer under a shear gas flow. *Interfacial Phenom. Heat Transf.* **2023**, *11*, 55–64. [CrossRef]
6. Shevchenko, V.; Mialdun, A.; Yasnou, V.; Lyulin, Y.V.; Ouerdane, H.; Shevtsova, V. Investigation of diffusive and optical properties of vapour-air mixtures: The benefits of interferometry. *Chem. Eng. Sci.* **2021**, *233*, 116433. [CrossRef]
7. McFadden, G.B.; Coriell, S.R. Onset of oscillatory convection in two liquid layers with phase change. *Phys. Fluids* **2009**, *21*, 034101. [CrossRef]
8. Lyubimova, T.; Lyubimov, D.; Parshakova, Y.; Ivantsov, A. Convection in a two-layer system with a deformable interface under low gravity conditions. *Microgravity Sci. Technol.* **2011**, *23*, 143–150. [CrossRef]
9. Liu, R.; Kabov, O.A. Instabilities in a horizontal liquid layer in cocurrent gas flow with an evaporating interface. *Phys. Rev. E* **2012**, *85*, 66305. [CrossRef] [PubMed]
10. Bekezhanova, V.B.; Goncharova, O.N. Stability of the exact solutions describing the two-layer flows with evaporation at interface. *Fluid Dyn. Res.* **2016**, *48*, 061408. [CrossRef]
11. Shefer, I.A. Influence of the Transverse Temperature Drop on the Stability of Two-Layer Fluid Flows with Evaporation. *Fluid Dyn.* **2019**, *54*, 603–613. [CrossRef]
12. Ostroumov, G.A. *Free Convection under the Conditions of an Internal Problem*; Gostekhizdat: Moscow, Russia; Leningrad, Russia, 1952; pp. 1–286. (In Russian)
13. Birikh, R.V. Thermocapillary convection in a horizontal layer of liquid. *J. Appl. Mech. Tech. Phys.* **1969**, *3*, 43–45. [CrossRef]
14. Pukhnachev, V.V. Theoretico-group nature of the Birikh's solution and its generalizations. In *Symmetry and Differential Equations, Proceedings of the International Conference "Symmetry and Differential Equations", Krasnoyarsk, Russia, 21–25 August 2000*; ICM SB RAS: Krasnoyarsk, Russia, 2000; pp. 180–183.
15. Nepomnyashchy, A.; Simanovskii, I.; Legros, J.C. *Interfacial Convection in Multilayer Systems*; Springer: New York, NY, USA, 2011; 498p.
16. Nepomnyashchy, A.A.; Velarde, M.G.; Colinet, P. *Interfacial Phenomena and Convection*; Chapman & Hall: Boca Raton, FL, USA, 2002; 365p.
17. Bekezhanova, V.B.; Goncharova, O.N. Theoretical analysis of the gravity impact on the parameters of flow regimes with inhomogeneous evaporation based on an exact solution of convection equations. *Microgravity Sci. Technol.* **2022**, *34*, 88. [CrossRef]
18. Andreev, V.K.; Gaponenko, Y.A.; Goncharova, O.N.; Pukhnachov, V.V. *Mathematical Models of Convection*; De Gruyter Studies in Mathematical Physics; De Gruyter: Berlin, Germany; Boston, MA, USA, 2012; 417p.
19. Pukhnachev, V.V. Group-theoretical methods in convection theory. *AIP Conf. Proc.* **2011**, *1404*, 27–38.
20. Stabnikov, V.N.; Royter, I.M.; Procyuk, T.B. *Ethyl Alcohol*; Food Industry: Moscow, Russia, 1976; 276p. (In Russian)
21. Weast, R.C.; Astle, M.J.; Beyer W.H. *CRC Handbook of Chemistry and Physics*, 64th ed.; CRC Press Inc.: Boca Raton, FL, USA, 1979; 2386p.
22. Godunov, S. On the numerical solution of boundary value problems for systems of ordinary linear equations. *Usp. Mat. Nauk* **1961**, *16*, 171–174. (In Russian)
23. Peng, C.-C.; Cerretani, C.; Braun, R.J.; Radke, C.J. Evaporation-driven instability of the precorneal tear film. *Adv. Colloid Interface Sci.* **2014**, *206*, 250–264. [CrossRef] [PubMed]
24. Tiwari, N.; Davis, J.M. Linear stability of a volatile liquid film flowing over a locally heated surface. *Phys. Fluids* **2009**, *21*, 022105. [CrossRef]
25. Kabov, O.A.; Zaitsev, D.V.; Cheverda, V.V.; Bar-Cohen, A. Evaporation and flow dynamics of thin, shear-driven liquid films in microgap channels. *Exp. Therm. Fluid Sci.* **2011**, *35*, 825–831. [CrossRef]